ACS OMEGA

Article

Cite This: ACS Omega 2018, 3, 11447−11454

http://pubs.acs.org/journal/acsodf

Key Role of the Local Hydrophobicity in the East Patch of Plastocyanins on Their Thermal Stability and Redox Properties

José Luis Olloqui-Sariego,*[,†] Inmaculada Márquez,[†] Estrella Frutos-Beltrán,[‡,§] Irene Díaz-Moreno,[‡] Miguel A. De la Rosa,[‡] Juan José Calvente,[†] Rafael Andreu,[†] and Antonio Díaz-Quintana*[,‡]

[†]Departamento de Química Física, Universidad de Sevilla, c/ Profesor García González, 1, 41012 Sevilla, Spain

[‡]Instituto de Investigaciones Químicas, cicCartuja, Universidad de Sevilla y CSIC, Avd. Américo Vespucio 49, 41092 Sevilla, Spain

ABSTRACT: Understanding the molecular basis of the thermal stability and functionality of redox proteins has important practical applications. Here, we show a distinct thermal dependence of the spectroscopic and electrochemical properties of two plastocyanins from the thermophilic cyanobacterium *Phormidium laminosum* and their mesophilic counterpart from *Synechocystis* sp. PCC 6803, despite the similarity of their molecular structures. To explore the origin of these differences, we have mimicked the local hydrophobicity in the east patch of the thermophilic protein by replacing a valine of the mesophilic plastocyanin by isoleucine. Interestingly, the resulting mutant approaches the thermal stability, redox thermodynamics, and dynamic coupling of the flexible site motions of the thermophilic protein, indicating the existence of a close connection between the hydrophobic packing of the east patch region of plastocyanin and the functional control and stability of the oxidized and reduced forms of the protein.

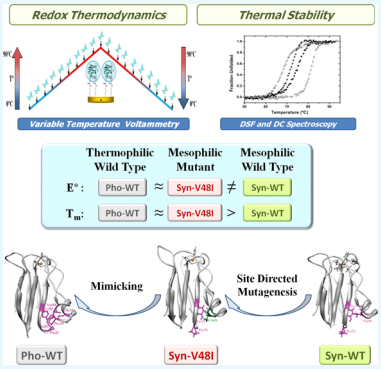

1. INTRODUCTION

Understanding the structural and molecular factors that modulate the thermal stability and activity of redox proteins is of high scientific and technological interest.[1−4] Plastocyanin (Pc) is a member of the blue copper protein family and acts as an electron carrier in oxygenic photosynthesis.[5] Despite their structural similarities, Pc from the thermophilic cyanobacterium *Phormidium laminosum* (*Pho*-Pc) displays a higher thermal stability than its counterpart from mesophilic *Synechocystis* sp. *PCC 6803* (*Syn*-Pc), as well as a different dependence of the melting point on the redox state.[6,7] Copper ligands are known to play a key role in the thermal stability of blue copper proteins,[2,8−10] and they are highly conserved in Pcs. On the other hand, molecular dynamics (MD) simulations suggest that small structural differences in the flexible loop L5 (see Figure 1) can modulate the stability of the active copper site and contribute to the protein's thermal response.[7,11] This loop is far from the copper center and takes part in the so-called east patch, also known as site 2 in functional analysis. Further, the triple mutant A44D/D49P/A62L of *Syn*-Pc,[12] designed by sequence comparison to stabilize the redox behavior of the protein during crystallization trials, displays a conformation of loop L5 similar to that found in the structure in the solution of the wild-type (WT) species (Figure 1).

This indirect control was evident when inducing a thermal destabilization of the thermophilic protein after introducing a single mutation in the east patch.[15] Further X-ray absorption spectroscopy investigations revealed that this mutation induces a subtle change in the local geometry of the Cu-binding site, which then causes the thermal stabilization.[16] Nevertheless, the mechanism that allows this flexible region, located far from the metal active center, to regulate the protein's thermal stability is not fully understood.

Here, we have investigated the thermostability and redox properties of Pcs by variable-temperature cyclic voltammetry and fluorescence and circular dichroism (CD) spectroscopic measurements. Notably, the thermophilic and mesophilic variants display different thermal dependence of the spectroscopic and electrochemical properties. To dig into the structural factors causing these differences, we have analyzed the effect of replacing the amino acid Val48 of *Syn*-Pc by isoleucine (V48I *Syn*-Pc). Considering that Val48 is located between loops L5 and L7 in the east patch of *Syn*-Pc, this mutation aims at stabilizing the mesophilic variant by introducing an extra methylene group between the two aforementioned loops, thereby trying to mimic the local hydrophobicity of the thermophilic variant (see Figure 1). The loops L1 and L5 are the areas with the highest fluctuations in all Pcs. In the vicinity of the L5 loop of *Syn*-Pc, there is a cavity in which two water molecules are intercalated that interact with the residues of the L5 and L7 loops and form a network of hydrogen bridges. The L5 loop has a three-residue insert that allows the formation of a hydrophobic cluster consisting of residues Phe80, Val48, Ile55, Pro81, Pro49, and Tyr85 in *Pho*-Pc. However, such grouping is reduced to Tyr79, Val48, and Pro76 in *Syn*-Pc. The inclusion of an extra methylene group by the substitution of valine 48 in *Syn*-Pc by an isoleucine is expected to reduce the gap between the L5 loop and the barrel, thereby increasing the hydrophobic interactions in the cluster,

Received: July 11, 2018
Accepted: September 6, 2018
Published: September 19, 2018

DOI: 10.1021/acsomega.8b01612
ACS Omega 2018, 3, 11447−11454

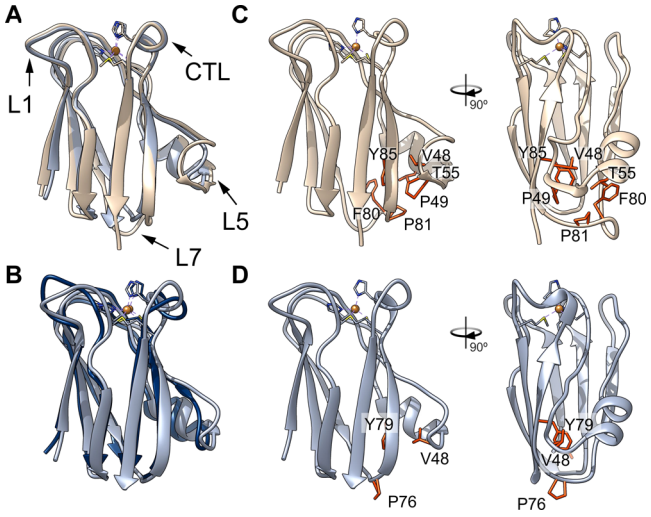

Figure 1. Comparison between the structures of *Phormidium* and *Synechocystis* Pcs. (A) Overlay of the X-ray diffraction structures of Pcs from *P. laminosum* (gray, pdb code 1baw[13]) and the triple mutant A44D/D49P/A62L (cyan, pdb code 1pcs; 12). The RMSD value for the backbone atoms is 0.77 Å. The arrows point to loops 1, 5, and 7, as well as the CTL, which contains three of the four metal ligands. (B) Overlay of the nuclear magnetic resonance structure of *Synechocystis* WT Pc (dark blue, pdb code 1jxd[14]) and the X-ray diffraction structure of the A44D/D49P/A62L mutant (cyan). The RMSD value for the backbone atoms is 0.86 Å. (C,D) Display of the residues involved in the interaction between loop L5 and the β barrel in *Phormidium* (C) and *Synechocystis* (D) Pcs from two perpendicular orientations. The side-chain bonds are represented in orange sticks.

decreasing its solvation, and reinforcing the van der Waals interactions among the residues in this area. The consequences of this mutation on the flexibility and mobility of the protein structure have been analyzed further by MD.

2. RESULTS AND DISCUSSION

2.1. Thermal Stability of Pcs. The thermal stabilities of oxidized and reduced Pcs are characterized by their melting points (T_m). The thermal stabilities of Pcs were investigated by monitoring the change in the intensity of fluorescence of tryptophan 31, a residue located within the hydrophobic pocket occluded by the east patch loop of Pc. The tryptophan fluorescence shift and intensity are, in fact, indicative of the exposure of its indol ring to the external aqueous environment.[17] Complementarily, CD was also used to detect the changes in the secondary structure during thermal unfolding. In particular, we followed the changes in the β-strand content upon increasing the temperature.[18] Figure 2 illustrates the normalized unfolding curves obtained by the fluorescence and CD measurements of the oxidized and reduced forms of the three Pcs. The normalized thermal unfolding curves were fitted to a simple two-state unfolding model[19] to estimate the melting points (T_m) of the Pcs according to the following equation

$$S = \frac{S_u + S_f\, e^{-\Delta G_f/RT}}{1 + e^{-\Delta G_f/RT}} \quad (1)$$

where S is the protein signal at a given temperature (T), S_u and S_f are the signals of protein solutions of equal concentration of either unfolded or folded protein, and ΔG_f is the free-energy difference of the equilibrium between the unfolded conformation and the native conformation. This free energy is approximated by the integrated Gibbs–Helmholtz equation

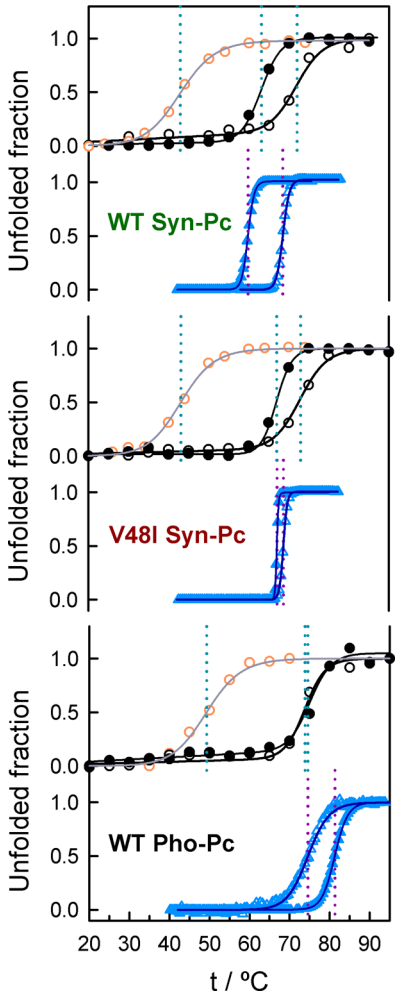

Figure 2. Thermal unfolding curves obtained by CD spectroscopy (circles) and fluorescence (triangles) of Pc species. The filled and open symbols (black and blue) correspond to the oxidized and reduced proteins, respectively. The open orange circles represent the CD data corresponding to the respective apoproteins. The lines are fits using a two-state equilibrium model.[19]

$$\Delta G_f = \Delta H_{T_m}\left(1 - \frac{T}{T_m}\right) - \Delta C_P\left[T_m - T + T\ln\left(\frac{T}{T_m}\right)\right] \quad (2)$$

where T_m, ΔH_{T_m}, and ΔC_P are the melting temperature, enthalpy change, and heat capacity change of the specific equilibrium, respectively. To fit the thermal unfolding curves of each Pc, we have simplified eq 2 by considering that $\Delta C_P \approx 0$, so that $\Delta G \approx \Delta H_{T_m}(1 - T/T_m)$. Moreover, we have considered that $S_f = S_f^0 + m_f(T - T_0)$ to account for the linear dependence of the CD signal of the folded protein prior to its thermal unfolding, where S_f^0 is the signal of native molecules at the low temperature T_0 and m_f is the slope of the spectroscopic signal showing a linear dependence with temperature.

The fitting parameters used to quantify the thermal unfolding curves of Pcs are listed in Table 1. The estimated T_m values of the oxidized and reduced forms of the protein by the two different spectroscopic techniques are somewhat

DOI: 10.1021/acsomega.8b01612
ACS Omega 2018, 3, 11447−11454

Table 1. Thermal Unfolding Parameters of Pcs

	WT Pho-Pc	*V48I Syn*-Pc	*WT Syn*-Pc
T_m (°C)/oxidized[a]	81.8 ± 0.4[c]	67.1 ± 0.1	59.8 ± 0.1
ΔH_{T_m} (kJ mol^{-1})/oxidized[a]	640 ± 50[c]	4500 ± 1000	1200 ± 500
T_m (°C)/reduced[a]	75.7 ± 1.0[c]	68.7 ± 0.3	68.5 ± 0.6
ΔH_{T_m} (kJ mol^{-1})/reduced[a]	380 ± 50[c]	2000 ± 1000	1200 ± 500
T_m (°C)/oxidized[b]	74.6 ± 0.5[c]	67.0 ± 0.7	63.1 ± 0.1
ΔH_{T_m} (kJ mol^{-1})/oxidized[b]	380 ± 30[c]	500 ± 50	380 ± 30
T_m (°C)/reduced[b]	73.9 ± 0.5[c]	73.8 ± 0.3	72.0 ± 0.3
ΔH_{T_m} (kJ mol^{-1})/reduced[b]	400 ± 50[c]	300 ± 30	300 ± 30
T_m (°C)/apo-Pc[b]	49.3 ± 1.3[c]	44.1 ± 0.3	43.4 ± 0.7
ΔH_{T_m} (kJ mol^{-1})/apo-Pc[b]	200 ± 30[c]	200 ± 30	200 ± 30

[a]Determined by fluorescence spectroscopy. [b]Determined by CD spectroscopy. [c]From refs 6 and 15.

different, but display similar qualitative trends (see Table 1). According to their T_m values, the oxidized form of *Pho*-Pc is more stable in solution than the reduced one, whereas the mesophilic variant shows the opposite trend, in agreement with previous works.[6,7,11,15] Interestingly, the V48I mutation increases the thermal stability of *Syn*-Pc. In particular, the oxidized V48I mutant is characterized by a higher T_m value than the oxidized *Syn*-Pc WT protein, whereas the T_m values of the reduced mutant and WT proteins were similar. This yields a smaller difference between the T_m values of the two redox forms in the mutant.

It should be noted that the normalized thermal unfolding curves obtained by the two different spectroscopic techniques for both oxidized and reduced forms of the three Pcs cannot be superimposed. These observations may indicate the presence of intermediate states at least in the Syn-Pc species. In fact, our data indicate that the regular structures disorder before Trp31 indol becomes accessible to the solvent. The opposite occurs for the oxidized *Pho*-Pc species. The larger slope of the CD curves is indicative of a high cooperativity, which involves the hydrogen bonds stabilizing the β-barrel fold. This agrees with the larger enthalpies coming out from our fits. Notably, the denaturation curves are systematically steeper for the reduced species, as compared to those of the oxidized forms. Such a behavior relates to the transition enthalpies and is expectable from the following facts. First, folding and denaturation of blue copper proteins are intimately linked to the formation or disruption of the copper site.[8,9,20] Second, the theoretical analyses have shown that the interactions of Cu(II) with its coordination sphere in blue copper proteins are more stabilizing than those involving Cu(I).[21]

To assign separate contributions of the protein matrix and the copper center to the thermal stabilization of V48I *Syn*-Pc, we have compared the T_m values of the apo and holo forms of the WT and mutant Pcs from *Synechocystis* (see Figure 2 and Table 1). The contribution of the protein matrix to protein stability is reflected in the T_m value of the apo-Pc, whereas the contribution of the copper center can be assessed by the T_m difference between the holo- and apoproteins. The T_m value of apo V48I *Syn*-Pc shows an increase of 0.7 °C compared to the value of apo *Syn*-Pc, which suggests a small effect of the mutation on the stability of the protein matrix itself. In fact, the T_m values for the oxidized and reduced forms of holo V48I *Syn*-Pc are 3.9 and 1.8 °C higher than that for *Syn*-Pc. Therefore, these results indicate that the thermal stability increase of the V48I *Syn*-Pc mutant is mainly related to the behavior of its copper center.

2.2. Redox Thermodynamics of Immobilized Pc. On the basis of the above findings, we have investigated the influence of the remote east patch region on the redox function of Pcs. In particular, we have assessed the temperature dependence of the interfacial electron transfer of immobilized Pcs on a cysteamine-modified gold electrode. To this end, the protein-modified electrode was subjected to a thermal cycle that lasted ∼6 h, where the temperature was first increased from 0 to 90 °C and then lowered back to 0 °C, while recording the cyclic voltammograms every 10 °C. Figure 3a illustrates some typical cyclic voltammograms recorded at 0 and 80 °C for the three Pcs. The thermodynamics of Pc redox conversion was characterized by its formal potential, which is determined as the midpoint potential ($E_{1/2}$) of the anodic and cathodic voltammetric waves at low scan rates. Figure 3b shows the temperature dependence of the midpoint potentials for the three Pcs. The temperature dependence of the $E_{1/2}$ values was found to be different for *Pho*-Pc and *Syn*-Pc. At low

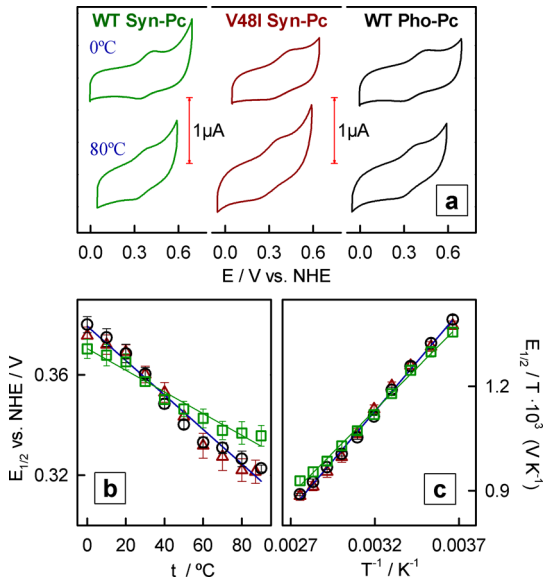

Figure 3. (a) Cyclic voltammograms recorded at the indicated temperatures and 0.05 V s^{-1} for immobilized Pcs. (b) $E_{1/2}$ vs T plots and (c) $E_{1/2}/T$ vs $1/T$ plots for immobilized *Pho*-Pc (black circle), *Syn*-Pc (green square), and *V48I Syn*-Pc (red triangle). Other experimental conditions: 0.1 M sodium phosphate buffer, pH 7. The error bars indicate the standard deviation of at least three replicated measurements for each data point.

DOI: 10.1021/acsomega.8b01612
ACS Omega 2018, 3, 11447−11454

temperatures, the $E_{1/2}$ values for *Pho*-Pc are more positive than for *Syn*-Pc, indicating a higher stabilization of the reduced *Pho*-Pc. However, as the temperature raises over 30 °C, the $E_{1/2}$ values of *Pho*-Pc become more negative than those of *Syn*-Pc, suggesting a further stabilization of the oxidized form of *Pho*-Pc as the temperature is increased.

The values of the redox thermodynamic parameters ΔS^0_{rc} and ΔH^0_{rc}, associated with the electron exchange between the protein and the electrode, were estimated from the slopes of the $E_{1/2}$ versus T (Figure 3b) and the $E_{1/2}/T$ versus $1/T$ (Figure 3c) plots, respectively, and are listed in Table 2. The

Table 2. Redox Thermodynamics of Immobilized Pcs

	WT Pho-Pc	*V48I Syn*-Pc	*WT Syn*-Pc
$E_{1/2,298K}$ (mV) vs NHE	369 ± 5	369 ± 5	365 ± 5
ΔS^0_{rc} (J mol^{-1} K^{-1})	−65 ± 4	−67 ± 9	−41 ± 7
ΔH^0_{rc} (kJ mol^{-1})	−54 ± 3	−54 ± 4	−47 ± 3

$E_{1/2}$ values for these proteins are found to be modulated by both enthalpic and entropic contributions. In particular, the redox thermodynamics of *Pho*-Pc and *Syn*-Pc is characterized by the highly negative ΔS^0_{rc} and ΔH^0_{rc} values, in agreement with previous results reported for the other proteins of the same family,[20−23] revealing significant differences in the protein solvation and/or structure upon changing its oxidation state. Thus, the larger absolute ΔS^0_{rc} and ΔH^0_{rc} values of *Pho*-Pc, as compared to those of *Syn*-Pc, would point to a higher flexibility of the protein matrix of *Pho*-Pc. Notably, the $E_{1/2}$ values of the V48I mutant are similar to those of the thermophilic protein in the whole temperature range we have explored (Figure 3b). The thermodynamic analysis of the $E_{1/2}$ values shows that the $E_{1/2}$ differences between the *Syn*-Pc mutant and its WT counterpart come from a competitive balance between the enthalpic and entropic contributions (see Table 2). These results reveal that the hydrophobic packing in the east patch region of Pc is crucial to control the relative stability and function of the oxidized and reduced forms of the protein.

Besides, the fact that the oxidized form of the V48I *Syn*-Pc mutant is more thermostable than the oxidized form of *Syn*-Pc, combined with the fact that the $E_{1/2}$ values of the V48I *Syn*-Pc mutant are negatively shifted, up to 20 mV at the highest temperature, suggests the existence of a relationship between the redox function and protein thermal stability.

2.3. MD of Pc. Bearing in mind that the thermostability and functionality of redox proteins are related to their structural flexibility,[24−28] we have analyzed the influence of the local hydrophobicity of the east patch of these Pcs on their mobility and flexibility by MD. We have performed a series of MD simulations at 298 K (see Figure 4).

The total simulated time was 50 ns in each run. This assures a sufficient conformation sampling, as we showed for *Pho*-Pc in the previous 10 ns computations.[29] The structure of the three proteins hardly changed along the computations, according to the behavior of the radius of gyration (R_G) and the RMS deviations (RMSD) of the backbone atom coordinates along the trajectories (Figure 4A). In fact, the RMSD between the average structure of the trajectories and the coordinates in the PDB (Protein Data Bank) were 1.04 Å for *Pho*-Pc (pdb code: 1baw) and 1.2 Å for *Syn*-Pc (pdb code: 1pcs), and the largest differences were located at the mobile loops L1 and L5. The analysis of the per-residue fluctuations carried out to test the flexibility of the different parts of the protein showed similar

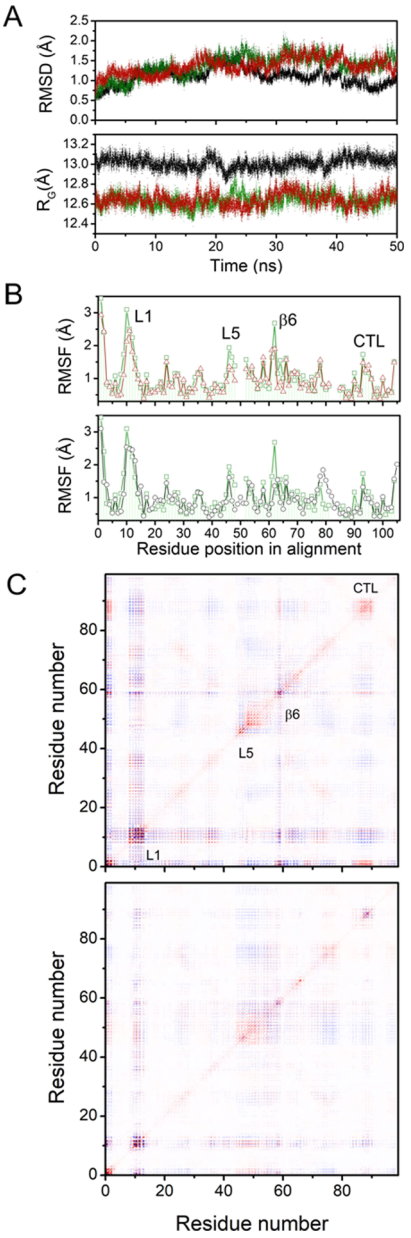

Figure 4. MD computations of Syn-Pc (green), V48I *Syn*-Pc (red), and *Pho*-Pc (black). (A) Time courses for the RMSD with respect to the energy-minimized structure and R_G. (B) Comparison of the per-residue atomic fluctuations computed as the root-mean-square (RMS) fluctuations with respect to the average coordinates. The residue numbering takes into account two three-residue insertions in the sequence of *Pho*-Pc, to make comparisons easier. (C) Comparison of $3N \times 3N$ covariance matrices for the coordinates of the C_α atoms of *Syn*-Pc (top) and V48I *Syn*-Pc (bottom). The negative values are in blue; positive in red. The two plots have the same intensity scale.

patterns for the three Pcs (Figure 4B). Nevertheless, *Syn*-Pc showed slightly higher values than the two other proteins for the three sequence stretches corresponding to the loops L1, L5, and the C-terminal loop (CTL), which provides three of the ligands to the metal. To test whether such minimal changes would have a functional meaning, the covariance matrix of atomic coordinates for *Syn*-Pc and the V48I mutant was obtained (Figure 4C). Notably there are substantial differences between the inter-residual covariances, suggesting a change in the coupling of motions of flexible regions within the proteins.

DOI: 10.1021/acsomega.8b01612
ACS Omega 2018, 3, 11447−11454

Then, the quasi-harmonic analysis of the mass-weighted covariance of main chain atoms allowed us to determine the concerted motions within the three proteins. Figure 5 displays the RMS fluctuation ellipsoids for the first nontrivial modes.

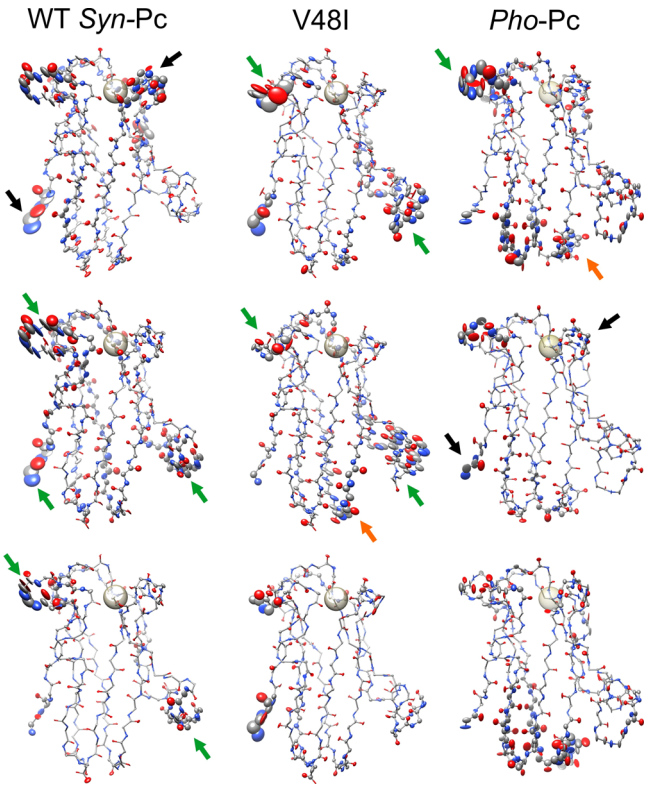

Figure 5. Thermal ellipsoids for the first internal motion modes of the main chain atoms. The ellipsoid amplitudes are proportional to the atomic fluctuations along the trajectory for each mode. The ellipsoid colors follow the CPK scheme of the corresponding atoms. The arrows highlight the differences in the coupling of the flexible site motions.

For *Syn*-Pc, this "essential dynamics" analysis shows a strong correlation of motions of the N-terminus with loops 1 and C (black arrows in Figure 5). This coupling of motions involving the CTL is much weaker for *Pho*-Pc and V48I *Syn*-Pc. This is also consistent with our previous analysis by X-ray absorption near-edge spectroscopy, showing a 0.15 Å increase in the Cu–$S\gamma_{Cys}$ bond length in the reduced *Syn*-Pc with respect to that in *Pho*-Pc.[16] Instead, both *Pho*-Pc and V48I *Syn*-Pc show an increased coupling between the motions of loop 1 and the other regions of the protein far from the copper site, including loop 5 in the east patch (green and orange arrows in Figure 5). These results strongly suggest a relationship between the coupling of the internal motions of the CTLs containing the copper ligands and the packing of the hydrophobic residues located in the east patch of Pc.

Question arises about the mechanisms underlying the coupling between loops L1, L5, and CTL. Given the stiffness of the β barrel, we were unable to find significant conformation changes in its internal residues, separating loop L5 in one of the poles of the molecule from loops L1 and CTL in the other. Most probably, the coupling mechanism may involve long-range interactions such as electrostatics. Indeed, the electrostatic fields around the three proteins differ, as shown in the surface potentials in Figure 6A. Two residues, a glutamic

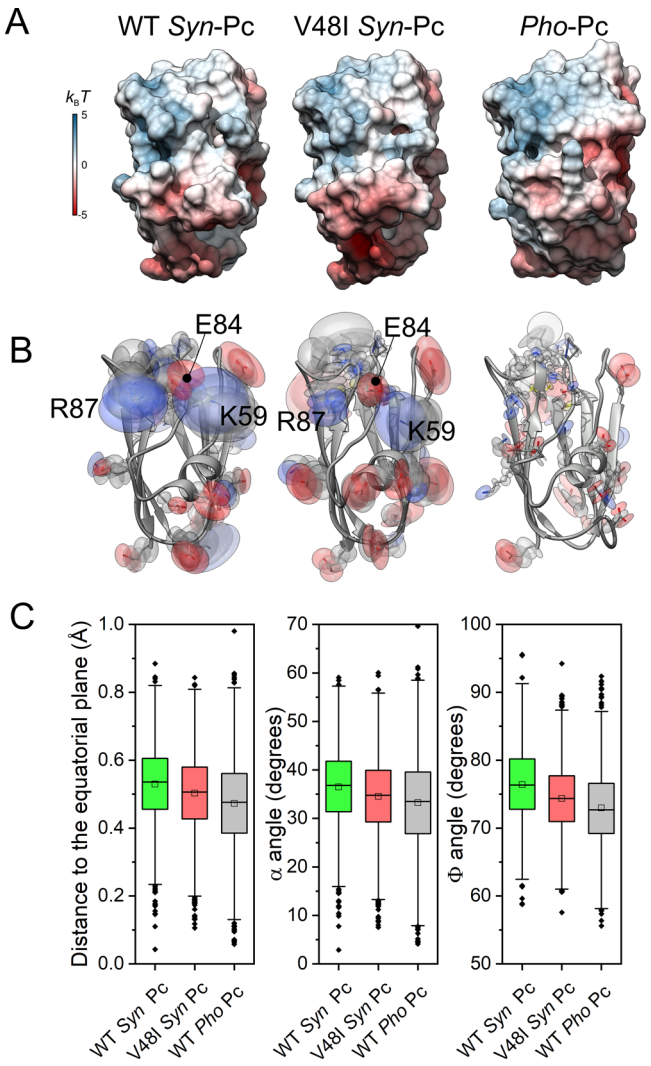

Figure 6. Side-chain effects of theV48I mutation. (A) Electrostatic potentials at the surface of oxidized WT *Syn*-Pc, V48I *Syn*-Pc, and *Pho*-Pc. (B) Thermal ellipsoids for the first internal motion mode of side chains of ionizable residues and amino acids near the copper site. Ellipsoid amplitudes are the atomic fluctuations along the trajectory for this mode. All atoms are colored according to the CPK profile. (C) Box diagrams corresponding to the MD-derived statistics of the geometrical parameters associated to the copper site properties at 25 °C, as described in the main text.

residue (E84) and an arginine one (R87; R93 in *Pho*-Pc) are located in the CTL. E84 is absent in *Pho*-Pc, for which remote mutations at L5 also impact the copper site, turning it into a *Syn*-Pc-like species.[15,16] However, E84 is involved in the network of salt bridges across the east side of the protein.[11] R87 is highly conserved in Pcs, and a 30 mV decrease in E_0' takes place upon the mutation of this residue in *Nostoc* Pc.[30] This residue points to the exposed region of the so-called east patch and, in *Syn*-Pc species, forms a salt bridge with E84.[11] Figure 6B illustrates how the V48I mutation decreases the interplay among K59, E84, and R87, and, as a result, the fluctuations in the side chain of R87 decrease. In *Pho*-Pc, R93 (R87 in *Syn* proteins) is restrained through its interaction with D44 (the average distance between the polar heads is ca. 6 Å). Moreover, Figure 6 also shows an overall change in the behavior of the rest of the charged residues, in particular those at the L5 loop, which may also influence the behavior of R87.

DOI: 10.1021/acsomega.8b01612
ACS Omega 2018, 3, 11447−11454

In agreement, the mutations in this region decrease the redox potential measured in solution, depending on their impact on the electrostatic potential.[31]

The observed changes affect the geometry of the first metal coordination sphere and its environment. Figure 6C displays the average of three parameters related to the stability and other properties of the oxidized copper site.[21,32] Cu(I) tends to form a trigonal planar geometry, whereas Cu(II) tends to form tetrahedral coordinates.[21] Thus, the height of Cu above the equatorial plane relates to the stability of the oxidized species. The other two parameters, the angle Φ between the N−Cu−N and S−Cu−S planes and the angle α between the N−Cu−N plane and the Cu−Sγ_{Cys} bond, relate to the overlap between the metal and ligand orbitals, again affecting the stability of the active site. Notably, we found small but significant differences (all p values in the Student t test below 10^{-19}) among the three proteins in these geometric parameters, V48I *Syn*-Pc displaying a value between those of WT *Syn*-Pc and *Pho*-Pc. Notably, according to these data, the oxidized form at 25 °C is less stable in the last one, in agreement with the slightly higher redox potential observed experimentally.

3. CONCLUSIONS

The comparison of the thermal and functional behaviors of a thermophilic Pc from *Phormidium laminosum* with that of its mesophilic counterpart from *Synechocystis* sp. *PCC 6803*, in a wide temperature range (0−90 °C), reveals a marked difference in their redox properties and thermal stability. A single point mutation, trying to replicate the local hydrophobicity of the thermophilic variant in the east patch, modifies significantly the melting point and redox parameter values, which become close to those of the thermophilic protein. Moreover, MD computations reveal similarities in the coupling of flexible site motions of *Pho*-Pc and V48I *Syn*-Pc that are not present in WT *Syn*-Pc, indicating that the observed behaviors correlate with the degree of coupling of the CTL motions to those of the remote hotspots of the protein. Such differences seem to originate from the changes in the coupling interactions between the ionizable side chains. These findings showcase the existence of a relationship between the structural properties of the hydrophobic cluster, located in the east patch region of Pc, and dynamic coupling of the flexible site motions and the relative stability and function of the oxidized and reduced forms of the protein.

4. EXPERIMENTAL SECTION

4.1. Protein Production. The expression of the petE genes from *Synechocystis* sp. and *P. laminosum*—using pBluescript II SK+ constructs already published—followed the procedures previously described.[6,7] Site-directed mutagenesis was performed with the "quick change" method (Stratagen Inc., La Jolla, CA, USA). The WT and V48I *Syn*-Pc proteins were produced in *Escherichia coli* DH5α strains, whereas the expression of the *Pho*-Pc coding gene took place in the electroporated K12 cells. As described previously, the proteins were purified by ion-exchange chromatography across a diethyl-aminoethyl cellulose column, using a 5 mM tris-(hydroxymethyl)aminomethane (Tris)/HCl buffer and a 10−180 mM NaCl concentration gradient. The WT and V48I *Syn*-Pc species were further purified by chromatofocusing in a Polybuffer Exchanger 94 (Sigma-Aldrich) column equilibrated in 5 mM Tris/acetate, pH 7.0, and a subsequent size exclusion step in Sephadex G50. In its turn, *Pho*-Pc purification required an additional size exclusion chromatography step in a HiLoad 16/60 Sephadex 75 (Pharmacia) column equilibrated in 100 mM NaCl and 10 mM sodium phosphate buffer, pH 7.0. The protein concentrations and purity were determined by measuring the light absorption at 280 nm (protein) and 597 nm (oxidized blue copper site), using a 4500 M^{-1} cm^{-1} extinction coefficient for the copper site at 597 nm.

4.2. Variable-Temperature Cyclic Voltammetry. Polycrystalline gold disk electrodes had a geometric area of 0.0314 cm^2. Prior to measurements, the gold surface was cleaned by successively polishing with 0.3 and 0.05 μm alumina and rinsed with Millipore water, and then it was sonicated in absolute ethanol to remove the residual alumina. The surface was then dried with argon and chemically cleaned using a "piranha" solution (7:3 mixture of concentrated H_2SO_4 and 30% H_2O_2). The cysteamine self-assembled monolayers were prepared by immersing the gold electrode in a 1 mM cysteamine solution in ethanol for 2 h at 4 °C. Protein immobilization was carried out by depositing onto the thiol-modified electrode surface of a 10 μL drop 100 μM protein Pc, 10 mM sodium phosphate buffer solution of pH 7 for 16 h at room temperature. Then, the electrodes were thoroughly rinsed with water and washed with the working buffer solution.

Linear scan voltammetric measurements were performed with an Autolab PGSTAT 30 from Eco Chemie B.V., in a three-electrode undivided glass cell, equipped with a gas inlet and thermostated with a water jacket. The counter and reference electrodes were a Pt bar and an Ag/AgCl/NaCl saturated electrode, respectively. The reference electrode was connected to the cell solution via a salt bridge and kept at room temperature (23 ± 2 °C) in a nonisothermal configuration. The reported potential values have been corrected to the normal hydrogen electrode (NHE) potential scale by adding +192 mV to the experimental potential values. All measurements were carried out under argon atmosphere. The working solutions contained 0.1 M sodium phosphate buffer at pH 7.0. To assess the influence of temperature on the midpoint potential, the electrode with the adsorbed protein was kept inside the electrochemical cell for ∼6 h, while the temperature was first increased from 0 to 90 °C, and then lowered back to 0 °C, with stops to record the voltammograms at different potential scan rates (from 0.01 to 0.1 V s^{-1}), every 10 °C.

4.3. Fluorescence Spectroscopy. The thermal titration curves derived from the fluorescence measurements were obtained according to the protocol described previously.[6] The measurements were performed with a Cary (Varian) fluorimeter coupled to a Polystat cc2 (Huber) bath for temperature control. The temperature of the sample was recorded using a Digitron 2008 system equipped with a flexible thermocouple that was inserted inside the cuvette and in contact with the sample. The protein concentration was 20 μM in a 10 mM pH 7 phosphate buffer solution. To maintain the protein in a single redox state throughout the experiment, equimolar concentrations of sodium ascorbate or potassium ferricyanide were added. The temperature in the cuvette was programmed to increase at a rate of 1 °C min^{-1}, from 20 to 95 °C. The sample was subjected to continuous stirring throughout the process to achieve temperature homogenization. The samples were excited with 275 nm light, and the fluorescence emission was monitored at 350 nm. As a control before and after each temperature ramp, an emission spectrum

DOI: 10.1021/acsomega.8b01612
ACS Omega 2018, 3, 11447−11454

from 300 to 600 nm was recorded, whereas the sample was being excited with a 275 nm ultraviolet light. The fluorescence and temperature data were recorded every 30 s and exported to the Origin Version 8.0 program for analysis.

4.4. CD Spectroscopy. To monitor the changes in the secondary structure during unfolding, the CD spectra were recorded in the far ultraviolet region (190−240 nm) with a Jasco J-815 spectropolarimeter, while increasing the temperature from 25 to 95 °C at a rate of 1 °C min^{-1} with a Peltier unit. Three spectra were recorded every 5 °C, with a scanning speed of 200 nm min^{-1}. The samples contained 15 μM protein in a 10 mM pH 7 phosphate buffer solution. The unfolding curves were obtained from the CD values recorded at 219 nm.

4.5. Computational Analysis. The MD trajectories were computed with the Amber 16 package,[33] using the 14SB force field,[34] except for the copper site for which the parameters set by Comba and Remenyi[35] and the restrained electrostatic potential charges computed by Muñoz-López[6] were applied. The simulations were run under periodic boundary conditions in orthorhombic boxes, wherein the initial minimum distance from the protein to cell faces was 10 Å. The particle mesh Ewald electrostatics was set with the Ewald summation cutoff at 9 Å. The counterions neutralized the charges of the system. The structures were solvated with SPC water molecules.[36] The protein side chains were energy-minimized (100 steepest descent and 1400 conjugate gradient steps) down to an RMS energy gradient of 0.01 kJ mol^{-1} $Å^{-1}$. Afterward, the solvent was subjected to 1000 steps of steepest descent minimization, followed by 500 ps *NPT*-MD computations using isotropic molecule position scaling and a pressure relaxation time of 2 ps at 298 K. The temperature was regulated with Berendsen's heat bath algorithm,[31] with a coupling time constant equal to 0.5 ps. The density of the system reached a plateau after ca. 150 ps simulation. Then, for each protein, the whole system was energy-minimized and submitted to *NVT*-MD at 298 K, using 2.0 fs integration time steps. The SHAKE algorithm[37] was used to constrain the bonds involving hydrogen atoms. The coordinate files were processed using CPPTRAJ.[38] Further processing was made in Origin 16 (Originlab), and the graphic displays were built in UCSF Chimera.[39] The electrostatic potentials were computed with the APBS software.[40]

AUTHOR INFORMATION

Corresponding Authors

*E-mail: jlolloqui@us.es (J.L.O.-S.).
*E-mail: qzaida@us.es (A.D.-Q.).

ORCID

José Luis Olloqui-Sariego: 0000-0002-3737-9814

Present Address

[§]Sygnis Pharma AG; Parque Científico de Madrid, c/ Faraday, 7, 28049 Madrid, Spain.

Notes

The authors declare no competing financial interest.

ACKNOWLEDGMENTS

J.L.O.-S., I.M., J.J.C., and R.A. acknowledge the financial support from the Spanish Ministry of Economy and Competitiveness and the European Union FEDER (grants CTQ2014-52641-P and CTQ2015-71955-REDT (ELECTROBIONET), I.D.-M., M.A.D.l.R., and A.D.-Q. thank funds from the Spanish Ministry of Economy, Industry and Competitiveness (BFU2015-71017/BMC), Ramon Areces Foundation (2015−2017), and the Andalusian Government (BIO-198). E.F.-B. was hired with funds from the Andalusian Government to A.D.-Q. (P06-CVI-01713).

REFERENCES

(1) Szilágyi, A.; Závodszky, P. Structural differences between mesophilic, moderately thermophilic and extremely thermophilic protein subunits: results of a comprehensive survey. *Structure* **2000**, *8*, 493−504.

(2) Chan, C.-H.; Yu, T.-H.; Wong, K.-B. Stabilizing salt-bridge enhances protein thermostability by reducing the heat capacity change of unfolding. *PLoS One* **2011**, *6*, No. e21624.

(3) Sen, S.; Nilsson, L. *Thermostable Proteins: Structural Stability and Design*; CRC Press, Taylor & Francis Group, LLC, 2012.

(4) Gromiha, M. M.; Pathak, M. C.; Saraboji, K.; Ortlund, E. A.; Gaucher, E. A. Hydrophobic environment is a key factor for the stability of thermophilic proteins. *Proteins: Struct., Funct., Bioinf.* **2013**, *81*, 715−721.

(5) Redinbo, M. R.; Yeates, T. O.; Merchant, S. Plastocyanin: structural and functional analysis. *J. Bioenerg. Biomembr.* **1994**, *26*, 49−66.

(6) Feio, M. J.; Navarro, J. A.; Teixeira, M. S.; Harrison, D.; Karlsson, B. G.; De la Rosa, M. A. A Thermal Unfolding Study of Plastocyanin from the Thermophilic CyanobacteriumPhormidium laminosum†. *Biochemistry* **2004**, *43*, 14784−14791.

(7) Feio, M. J.; Díaz-Quintana, A.; Navarro, J. A.; De la Rosa, M. A. Thermal Unfolding of Plastocyanin from the Mesophilic CyanobacteriumSynechocystissp. PCC 6803 and Comparison with Its Thermophilic Counterpart fromPhormidium laminosum†. *Biochemistry* **2006**, *45*, 4900−4906.

(8) Pozdnyakova, I.; Wittung-Stafshede, P. Biological relevance of metal binding before protein folding. *J. Am. Chem. Soc.* **2001**, *123*, 10135−10136.

(9) Pozdnyakova, I.; Guidry, J.; Wittung-Stafshede, P. Probing copper ligands in denatured Pseudomonas aeruginosa azurin: Unfolding His117Gly and His46Gly mutants. *J. Biol. Inorg Chem.* **2001**, *6*, 182−188.

(10) Alcaraz, L. A.; Donaire, A. Rapid binding of copper(I) to folded aporusticyanin. *FEBS Lett.* **2005**, *579*, 5223−5226.

(11) Muñoz-López, F. J.; Raugei, S.; De la Rosa, M. A.; Díaz-Quintana, A. J.; Carloni, P. Changes in non-core regions stabilise plastocyanin from the thermophilic cyanobacterium Phormidium laminosum. *J. Biol. Inorg Chem.* **2010**, *15*, 329−338.

(12) Bond, C. S.; Bendall, D. S.; Freeman, H. C.; Guss, J. M.; Howe, C. J.; Wagner, M. J.; Wilce, M. C. J. The structure of plastocyanin from the cyanobacterium Phormidium laminosum. *Acta Crystallogr., Sect. D: Biol. Crystallogr.* **1999**, *55*, 414−421.

(13) Romero, A.; De la Cerda, B.; Varela, P. F.; Navarro, J. A.; Hervás, M.; De la Rosa, M. A. The 2.15 Å crystal structure of a triple mutant plastocyanin from the cyanobacterium Synechocystis sp. PCC 6803 1 1Edited by R. Huber. *J. Mol. Biol.* **1998**, *275*, 327−336.

(14) Bertini, I.; Bryant, D. A.; Ciurli, S.; Dikiy, A.; Fernández, C. O.; Luchinat, C.; Safarov, N.; Vila, A. J.; Zhao, J. Backbone Dynamics of Plastocyanin in Both Oxidation States. *J. Biol. Chem.* **2001**, *276*, 47217−47226.

(15) Muñoz-López, F. J.; Beltrán, E. F.; Díaz-Moreno, S.; Díaz-Moreno, I.; Subías, G.; De la Rosa, M. A.; Díaz-Quintana, A. Modulation of copper site properties by remote residues determines the stability of plastocyanins. *FEBS Lett.* **2010**, *584*, 2346−2350.

(16) Chaboy, J.; Díaz-Moreno, S.; Díaz-Moreno, I.; De la Rosa, M. A.; Díaz-Quintana, A. How the Local Geometry of the Cu-Binding Site Determines the Thermal Stability of Blue Copper Proteins. *Chem. Biol.* **2011**, *18*, 25−31.

(17) Royer, C. A. Probing protein folding and conformational transitions with fluorescence. *Chem. Rev.* **2006**, *106*, 1769−1784.

DOI: 10.1021/acsomega.8b01612
ACS Omega 2018, 3, 11447−11454

(18) Greenfield, N. J. Using circular dichroism collected as a function of temperature to determine the thermodynamics of protein unfolding and binding interactions. *Nat. Protoc.* **2007**, *1*, 2527−2535.
(19) Sancho, J. The stability of 2-state, 3-state and more-state proteins from simple spectroscopic techniques... plus the structure of the equilibrium intermediates at the same time. *Arch. Biochem. Biophys.* **2013**, *531*, 4−3.
(20) Wittung-Stafshede, P. Role of cofactors in folding of the blue-copper protein azurin. *Inorg. Chem.* **2004**, *43*, 7926−7933.
(21) Pavelka, M.; Burda, J. V. Computational study of redox active centres of blue copper proteins: a computational DFT study. *Mol. Phys.* **2008**, *106*, 2733−2748.
(22) Battistuzzi, G.; Borsari, M.; Loschi, L.; Righi, F.; Sola, M. Redox Thermodynamics of Blue Copper Proteins. *J. Am. Chem. Soc.* **1999**, *121*, 501−506.
(23) Battistuzzi, G.; Bellei, M.; Borsari, M.; Canters, G. W.; de Waal, E.; Jeuken, L. J. C.; Ranieri, A.; Sola, M. Control of Metalloprotein Reduction Potential: Compensation Phenomena in the Reduction Thermodynamics of Blue Copper Proteins†. *Biochemistry* **2003**, *42*, 9214−9220.
(24) Radestock, S.; Gohlke, H. Exploiting the Link between Protein Rigidity and Thermostability for Data-Driven Protein Engineering. *Eng. Life Sci.* **2008**, *8*, 507−522.
(25) Teilum, K.; Olsen, J. G.; Kragelund, B. B. Functional aspects of protein flexibility. *Cell. Mol. Life Sci.* **2009**, *66*, 2231−2247.
(26) Radestock, S.; Gohlke, H. Protein rigidity and thermophilic adaptation. *Proteins: Struct., Funct., Bioinf.* **2011**, *79*, 1089−1108.
(27) Teilum, K.; Olsen, J. G.; Kragelund, B. B. Protein stability, flexibility and function. *Biochim. Biophys. Acta, Proteins Proteomics* **2011**, *1814*, 969−976.
(28) Karshikoff, A.; Nilsson, L.; Ladenstein, R. Rigidity versus flexibility: the dilemma of understanding protein thermal stability. *FEBS J.* **2015**, *282*, 3899−3917.
(29) Díaz-Moreno, I.; Muñoz-López, F. J.; Frutos-Beltrán, E.; De la Rosa, M. A.; Díaz-Quintana, A. Electrostatic strain and concerted motions in the transient complex between plastocyanin and cytochrome *f* from the cyanobacterium *Phormidium laminosum*. *Bioelectrochemistry* **2009**, *77*, 43−52.
(30) Molina-Heredia, F. P.; Hervás, M.; Navarro, J. A.; De la Rosa, M. A. A Single Arginyl Residue in Plastocyanin and in Cytochromec6from the CyanobacteriumAnabaenasp. PCC 7119 Is Required for Efficient Reduction of Photosystem I. *J. Biol. Chem.* **2001**, *276*, 601−605.
(31) De la Cerda, B.; Navarro, J. A.; Hervás, M.; De la Rosa, M. A. Changes in the Reaction Mechanism of Electron Transfer from Plastocyanin to Photosystem I in the CyanobacteriumSynechocystissp. PCC 6803 As Induced by Site-Directed Mutagenesis of the Copper Protein†. *Biochemistry* **1997**, *36*, 10125−10130.
(32) Donaire, A.; Jiménez, B.; Fernández, C. O.; Pierattelli, R.; Niizeki, T.; Moratal, J.-M.; Hall, J. F.; Kohzuma, T.; Hasnain, S. S.; Vila, A. J. Metal−Ligand Interplay in Blue Copper Proteins Studied by1H NMR Spectroscopy: Cu(II)−Pseudoazurin and Cu(II)−Rusticyanin. *J. Am. Chem. Soc.* **2002**, *124*, 13698−13708.
(33) Case, D. A.; Cheatham, T. E., III; Darden, T.; Gohlke, H.; Luo, R.; Merz, K. M., Jr.; Onufriev, A.; Simmerling, C.; Wang, B.; Woods, R. J. The Amber Biomolecular Simulation Programs. *J. Comput. Chem.* **2005**, *26*, 1668−1688.
(34) Maier, J. A.; Martinez, C.; Kasavajhala, K.; Wickstrom, L.; Hauser, K. E.; Simmerling, C. ff14SB: Improving the accuracy of protein side chain and backbone parameters from ff99SB. *J. Chem. Theory Comput.* **2015**, *11*, 3696−3713.
(35) Comba, P.; Remenyi, R. A new molecular mechanics force field for the oxidized form of blue copper proteins. *J. Comput. Chem.* **2002**, *23*, 697−705.
(36) Berendsen, H. J. C.; Postma, J. P. M.; van Gunsteren, W. F.; DiNola, A.; Haak, J. R. Molecular dynamics with coupling to an external bath. *J. Chem. Phys.* **1984**, *81*, 3684−3690.
(37) Ryckaert, J.-P.; Ciccotti, G.; Berendsen, H. J. C. Numerical integration of the cartesian equations of motion of a system with constraints: molecular dynamics of n-alkanes. *J. Comput. Phys.* **1977**, *23*, 327−341.
(38) Roe, D. R.; Cheatham, T. E., 3rd PTRAJ and CPPTRAJ: Software for Processing and Analysis of Molecular Dynamics Trajectory Data. *J. Chem. Theory Comput.* **2013**, *9*, 3084−3095.
(39) Pettersen, E. F.; Goddard, T. D.; Huang, C. C.; Couch, G. S.; Greenblatt, D. M.; Meng, E. C.; Ferrin, T. E. UCSF Chimera-A visualization system for exploratory research and analysis. *J. Comput. Chem.* **2004**, *25*, 1605−1612.
(40) Baker, N. A.; Sept, D.; Joseph, S.; Holst, M. J.; McCammon, J. A. Electrostatics of nanosystems: application to microtubules and the ribosome. *Proc. Natl. Acad. Sci. U.S.A.* **2001**, *98*, 10037−10041.

DOI: 10.1021/acsomega.8b01612
ACS Omega 2018, 3, 11447−11454